Grazing-incidence x-ray photoelectron spectroscopy from multilayer media: Oxidized GaAs(100) as a case study

M. J. Chester* and Terrence Jach

Surface and Microanalysis Science Division, National Institute of Standards and Technology, Gaithersburg, Maryland 20899

At the energies of interest in x-ray photoelectron spectroscopy (XPS), total external reflection of the x-ray beam occurs from a smooth surface at small incidence angles. The penetration of the x rays into the material is strongly attenuated at these angles and surface sensitivity is enhanced in the XPS yields. As the incidence angle is increased, the x rays penetrate more deeply into the material and the XPS signal contains a larger contribution from the bulk. By exploiting this angle-dependent x-ray penetration depth, it is possible to obtain depth-dependent XPS spectra from which the concentration profiles of the photoelectron-emitting atoms can be inferred. In this paper we develop a general formalism for calculating grazing-incidence XPS (GIXPS) yields from multilayer media. A quantitative analysis of GIXPS spectra acquired from an oxidized GaAs(100) surface that was annealed to remove oxidized As will be discussed. The results show that this annealed oxide is composed of Ga_2O_3 and that the oxide-GaAs substrate interface is rough.

I. INTRODUCTION

X-ray photoelectron spectroscopy (XPS) is a well-established technique for chemical characterization of surfaces and thin films ($\lesssim 100$ Å) that has been used extensively as a probe of composition, chemical bonding state, and contamination. Surface sensitivity in typical XPS experiments is a result of the relatively short inelastic mean free paths (IMFP's) of electrons in matter, generally between 10 and 50 Å. While the IMFP's of the electrons are short compared to the x-ray attenuation lengths, they are sufficiently long that there is a significant contribution to the photoelectron signal from the subsurface region. To determine the homogeneity of a surface region or possible intermixing between media, the contributions to the photoelectron yields from different depths must be determined. One means that is commonly employed to this end is to vary the photoelectron detection angle, either by rotating the sample or moving the detector. Due to the increased electron attenuation with increased path length, photoelectrons collected at large takeoff angles (measured relative to the sample normal) or more surface sensitive than those collected at small angles.[1-3] Thus, by varying the electron detection angle, it is possible to enhance or decrease selectively the surface contributions to the photoelectron yields, thereby enabling one to infer the concentration profiles of the photoelectron emitting atoms.

One can also exploit the angle dependence of the x-ray penetration depth at small incidence angles (measured relative to the sample plane) to obtain depth-dependent XPS spectra.[4-8] At XPS x-ray energies, typically 500–1500 eV, the refractive indices of materials are slightly less than unity so that a beam of x rays incident on a flat surface at small incidence angles undergoes total external reflection. For incidence angles in this region, generally less than 3°, only an evanescent wave propagates within the medium and the x-ray attenuation lengths can become comparable to the IMFP's of photoelectrons.[4] At x-ray incidence angles larger than the angles for total external reflection, the x rays penetrate deep into the material, on the order of 10^4 Å.

In this paper we will present a general formalism for modeling grazing-incidence XPS (GIXPS) data from multilayer dielectric media. The algorithm developed for computing grazing-incidence photoelectron yields from surfaces and thin films closely parallels the theories of grazing-incidence reflectivity[9] and x-ray fluorescence[10] from multilayer media. After the theory is introduced, the model will be applied to study an oxidized GaAs. The oxide surface of interest is a UV oxidized GaAs(100) surface that has been annealed to thermally desorb the oxidized As. This system provides an excellent test of the theory and modeling of the data, as well as pointing out the strengths and limitations inherent with GIXPS.

II. THEORY

A. Electromagnetic fields in multilayer media

The notation employed for describing the interaction of electromagnetic radiation (x rays) with multilayer media is illustrated in Fig. 1. Medium 0 is defined to be vacuum and media 1 through N are dielectric layers of thickness Δ_j and refractive index n_j. Without loss of generality we will take the scattering plane to be $(x0z)$, and the wave vectors will be written as $\mathbf{k}_j^\pm = k_{jx}\hat{\mathbf{x}} \pm k_{jz}\hat{\mathbf{z}}$. In this expression, and in those that follow, a plus superscript denotes wave vectors, or electromagnetic fields, that are transmitted, i.e., refracted, into the medium while a minus sign denotes radiation that is reflected from an interface. It will be assumed that all boundaries
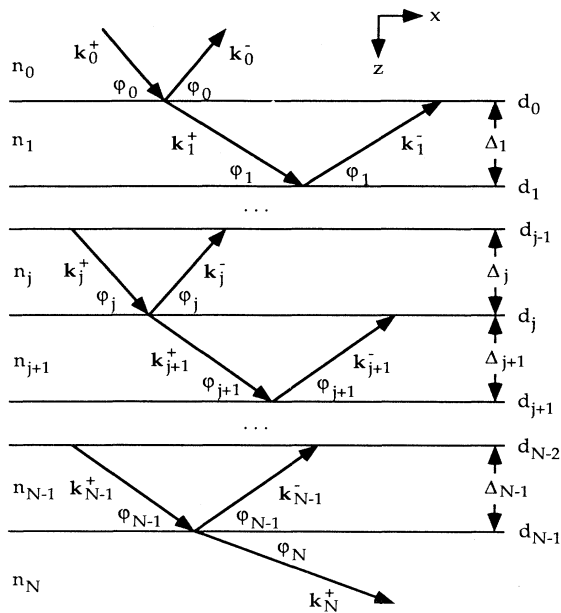
FIG. 1. Illustration of the model employed to calculate GIXPS yields from an arbitrary number of dielectric media.

between the dielectric media are perfectly planar and that the media are linear, isotropic, and free of sources. With these assumptions and simplifications, the solutions to Maxwell's equations are plane waves and the fields within a given medium can be written as a superposition of transmitted and reflected fields. The electric field in the jth medium may therefore be written as

$$\mathbf{E}_j(\mathbf{r},t)=\mathbf{E}_j^+(\mathbf{r},t)+\mathbf{E}_j^-(\mathbf{r},t) \ , \tag{1}$$

where

$$\mathbf{E}_j^\pm(\mathbf{r},t)=\mathbf{E}_j^\pm e^{\,i(\omega_j t-\mathbf{k}_j^\pm\cdot\mathbf{r})} \ . \tag{2}$$

By inserting these expressions into Maxwell's equations, it is straightforward to show that the wave-vector amplitudes $k_j^\pm$ and frequency ω_j are related to the material constants of the layer by the relation

$$k_j^\pm=\sqrt{\varepsilon_j\mu_j}\,\frac{\omega_j}{c} \ , \tag{3}$$

where ε_j is the dielectric constant at ω_j, μ_j is the permeability, and c is the speed of light in vacuum. Since the permeability differs negligibly from unity for most materials at XPS x-ray energies, we will assume that $\mu_j\equiv 1$ in the expressions that follow.[11] The index of refraction in layer j is then given by the expression

$$n_j=\sqrt{\varepsilon_j} \ . \tag{4}$$

At XPS x-ray energies, the dielectric function is only slightly less than unity. Defining the susceptibility as $\chi_j=1-\varepsilon_j$, it can be shown from the theory of dispersion that[12,13]

$$\chi_j=\frac{4\pi r_e}{k_j^2}\rho_j\sum_m x_{jm}(f_{m1}+if_{m2}) \ , \tag{5}$$

where r_e is the classical electron radius (2.82×10^{-13} cm) and ρ_j is the number density of molecular groups with x_{jm} atoms having real and imaginary atomic scattering factors f_{m1} and f_{m2}, respectively. Henke et al. have tabulated f_1 and f_2 for the elements at the more commonly used XPS energies.[13] Using these tables and Eq. (5), one finds that the real (χ_j') and imaginary (χ_j'') components of χ_j are in the range $10^{-5}-10^{-3}$.

The presence of boundary conditions between two media that must be satisfied for all points at the interface at all times implies that the frequencies and tangential components of the wave vectors are the same on both sides of the interface, i.e., $\omega_{j+1}=\omega_j$ and $k_{j+1x}=k_{jx}$. Extrapolating these results back to the vacuum-surface interface implies that

$$\omega_j=\omega_0 \ , \tag{6a}$$

$$k_{jx}=k_0\cos\phi_0 \ , \tag{6b}$$

and

$$k_{jz}=k_0\sqrt{\varepsilon_j-\cos^2\phi_0} \ , \tag{6c}$$

where we have set $\varepsilon_0=1$, the vacuum value of the dielectric function. Equations (6a), (6b), and (6c) reveal that the spatial and time dependence of the electric fields within the different media are completely determined by the energy and direction of the incident radiation and the dielectric functions of the layers.

A convenient measure of the angle below which the incident radiation is strongly attenuated within the sample is the critical angle for total external reflection ϕ_c. This angle is generally defined to be the angle at which the real part of the radicand in Eq. (6c) is equal to zero, i.e., $\mathrm{Re}\{\varepsilon_j\}=\cos^2\phi_c$. Since $\mathrm{Re}\{\varepsilon_j\}$ is only slightly smaller than unity, the small angle expansion of the cosine function can be used to show that $\phi_c\approx\sqrt{\chi_j'}$. For x-ray incidence angles smaller than ϕ_c, $\mathrm{Re}\{\varepsilon_j\}$ is negative and k_{1z} would be pure imaginary in the absence of an imaginary component to the dielectric function.

It is useful to decompose k_{jz} into real and imaginary components

$$k_{jz}=k_{jz}'-ik_{jz}'' \ . \tag{7}$$

The minus sign preceding the imaginary component is chosen as a matter of convenience so that k_{jz}' and k_{jz}'' are both positive numbers. Displayed in Fig. 2 are the real and imaginary components of the normal wave vector as a function of incidence angle for Mg $K\alpha$ radiation impinging on GaAs. The intersection of the two curves at 27 mrad is the critical angle. The imaginary component dominates at small incidence angles, whereas for incidence angles larger than the critical angle (such as in a typical XPS experiment) $k_{jz}''\ll k_{jz}'$. The consequence of considerable imaginary wave-vector components at incidence angles below the critical angle is that the refracted electric fields are more strongly attenuated at these angles than at larger incidence angles. This is easily seen by
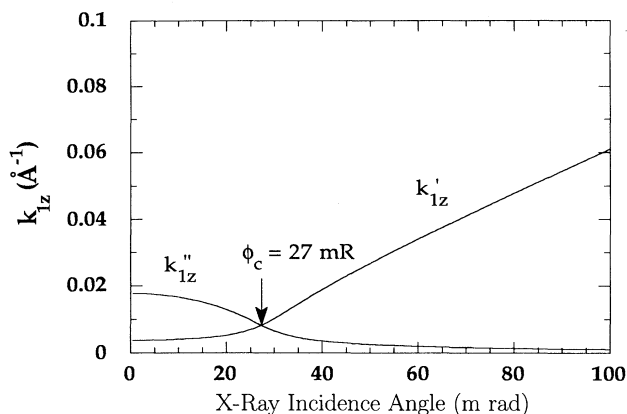
FIG. 2. Real and imaginary components of the wave vector normal to the surface for Mg $K\alpha$ radiation (1254 eV) incident on GaAs as a function of incident x-ray angle.

inserting Eqs. (6) and (7) into Eq. (2):

$$\mathbf{E}_j^{\pm}(\mathbf{x},t)=\mathbf{E}_j^{\pm}e^{i(\omega_0 t-k_{0x}x-k'_{jz}z)}e^{-k''_{jz}z} \ . \tag{8}$$

Having specified the wave vectors within the different dielectric layers, the electric-field strengths, and subsequently the field intensities, can be determined in each layer. The field amplitudes $\mathbf{E}_j^{\pm}$ are determined by satisfying the boundary conditions on the electric and magnetic fields. Generally one decomposes the fields into components that are perpendicular (σ polarization) and parallel (π polarization) to the plane of incidence. For GIXPS, however, the x-ray incidence angles are sufficiently small that the field amplitudes for each polarization state are essentially identical. It is therefore sufficient to restrict the discussion to the algebraically simpler of the two polarization states, namely, σ polar-

ization.

Before developing a general formalism for an N-layer film, it is instructive to examine the interaction of an x-ray beam with a single medium. For this problem there is no reflected radiation in the medium, i.e., $E_1^- \equiv 0$, and only the reflected field from the surface E_0^- and the transmitted field E_1^+ need to be determined. Continuity of the tangential electric and magnetic fields yields the following set of coupled equations:

$$E_0^+ + E_0^- = E_1^+ \ , \tag{9a}$$

$$s_0 E_0^+ - s_0 E_0^- = s_1 E_1^+ \ , \tag{9b}$$

where we have defined $s_j = n_j \sin\phi_j$ in anticipation of the more general problem. The solutions to these equations are the Fresnel reflection and transmission coefficients

$$r_{0,1} = \frac{E_0^-}{E_0^+} = \frac{s_0 - s_1}{s_0 + s_1} \tag{10a}$$

$$t_{0,1} = \frac{E_1^+}{E_0^+} = \frac{2s_0}{s_0 + s_1} \ . \tag{10b}$$

The generalization of the above discussion to multilayer media requires the inclusion of reflected components at the interfaces. Continuity of the tangential components of the electric and magnetic fields at an interface between layers j and $j+1$ yields the relations

$$E_j^+ e^{-ik_{jz}d_j}+E_j^- e^{ik_{jz}d_j}=E_{j+1}^+ e^{-ik_{j+1z}d_j}+E_{j+1}^- e^{ik_{j+1z}d_j} \tag{11a}$$

and

$$s_j E_j^+ e^{-ik_{jz}d_j}-s_j E_j^- e^{ik_{jz}d_j}=s_{j+1}E_{j+1}^+ e^{-ik_{j+1z}d_j}$$
$$-s_{j+1}E_{j+1}^- e^{ik_{j+1z}d_j} \ . \tag{11b}$$

These equations can be written in matrix form

$$\begin{bmatrix} 1 & 1 \\ s_j & -s_j \end{bmatrix}\begin{bmatrix} e^{-ik_{jz}d_j}E_j^+ \\ e^{ik_{jz}d_j}E_j^- \end{bmatrix} = \begin{bmatrix} 1 & 1 \\ s_{j+1} & -s_{j+1} \end{bmatrix}\begin{bmatrix} e^{-ik_{j+1z}d_j}E_{j+1}^+ \\ e^{ik_{j+1z}d_j}E_{j+1}^- \end{bmatrix} \ . \tag{12}$$

To compute the field intensities, and subsequently the photoelectron yields, the electric-field amplitudes $E_j^{\pm}$ need to be determined. To this end, Eq. (12) can be manipulated into the expression

$$\begin{bmatrix} E_j^+ \\ E_j^- \end{bmatrix} = \frac{1}{t_{j,j+1}}\begin{bmatrix} e^{i(k_{jz}-k_{j+1z})d_j} & r_{j,j+1}e^{i(k_{jz}+k_{j+1z})d_j} \\ r_{j,j+1}e^{-i(k_{jz}+k_{j+1z})d_j} & e^{-i(k_{jz}-k_{j+1z})d_j} \end{bmatrix}\begin{bmatrix} E_{j+1}^+ \\ E_{j+1}^- \end{bmatrix} \ , \tag{13}$$

where the Fresnel reflection ($r_{j,j+1}$) and transmission ($t_{j,j+1}$) coefficients are as defined by Eqs. (10a) and (10b) with the appropriate substitution of subscripts.

Equation (13) can be solved for all of the electric-field vectors $E_j^{\pm}$ in terms of the incident field amplitude E_0^+ by working backwards from the Nth dielectric layer. For this layer, E_N^- is identically equal to zero since radiation

is only transmitted through the medium. With $E_N^- = 0$, E_{N-1}^+ and E_{N-1}^- can be expressed in terms of E_N^+. Equation (13) can then be used to determine the fields in each of the remaining overlayers in terms of E_N^+. At the vacuum-surface interface this expression can be inverted to express E_N^+ in terms of the incident field amplitude E_0^+, which can then be substituted back into Eq. (13) to

solve for all of the fields in terms of the incident field amplitude E_0^+.

B. Grazing-incidence XPS from a single medium

Calculation of the photoelectron yields from a single medium as a function of incidence angle has been reported by Henke.[4] The yield of q-type photoelectrons is proportional to the electric-field intensity, the differential cross section for scattering q-type photoelectrons into the detector $d\sigma_q/d\Omega$, the density of photoelectron emitters, ρ_q, and the probability of electrons escaping from the sample in the no-loss peak. Electron attenuation will be modeled with an exponential decay that is characterized by an energy-dependent IMFP λ_q. Neglecting elastic scattering and photoelectron diffraction, the photoelectron flux that is collected in a spectrometer of small, constant solid angle Ω_d acting over the projection of an effective aperture area A_d onto the surface of a single medium may be written as[3]

$$dN_q(\phi_0,\theta,z) = \left[I_0 \frac{|E_1^+(z)|^2}{|E_0^+(z)|^2} \right] \left[\frac{d\sigma_q}{d\Omega}\Omega_d \right]$$

$$\times \left[\rho_{1q} \frac{A_d}{\cos\theta} \right] e^{-z/(\lambda_q \cos\theta)} D(E_e,E_p)dz \ ,$$

(14)

where I_0 is the incident photon flux density and $D(E_e,E_p)$ is an instrument-dependent function that contains the spectrometer transmission and detection efficiency of photoelectrons with incident kinetic energy E_e and spectrometer pass energy E_p. Using Eqs. (8) and (10b), this expression reduces to

$$dN_q(\phi_0,\theta,z) = \frac{I_0\Omega_d A_d}{\cos\theta} D(E_e,E_p)|t_{0,1}|^2$$

$$\times \left[\frac{d\sigma_q}{d\Omega} \right] \rho_{1q} e^{-(2k''_{1z}+\Lambda_q)z} dz \ ,$$

(15)

where $\Lambda_q = 1/(\lambda_q\cos\theta)$.

All of the depth dependence of the photoelectron yields is contained in the exponential term of Eq. (15). It is useful to define an angle-dependent GIXPS depth $d_{\gamma e}$ such that the contribution to the total yield at depth $d_{\gamma e}$ is $1/e$ of its value at the surface:[8]

$$d_{\gamma e} = \frac{1}{2k''_{1z}+\Lambda_q} \ .$$

(16)

This expression depends on both the x-ray incidence angle and the electron detection angle. For incidence angles larger than the critical angle, the x rays penetrate deep into the material and $d_{\gamma e} \approx \lambda_q\cos\theta$, the characteristic no-loss photoelectron escape depth. Depending upon the photoelectron energy and the sample material, the x-ray penetration depth can become comparable to the characteristic no-loss electron escape depth. GIXPS depths for Mg $K\alpha$ radiation incident on a GaAs surface at two commonly used detection angles are plotted in Fig. 3. An electron IMFP of 26 Å was used for both Ga
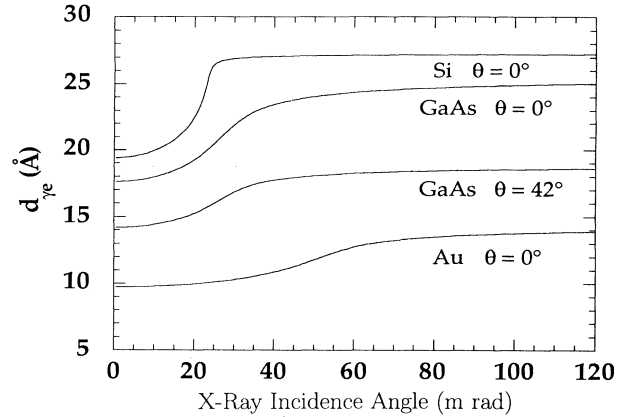
FIG. 3. Characteristic GIXPS depths for Mg $K\alpha$ radiation incident on Si, GaAs, and Au at electron detection angles normal to the surface. These depths are for Si $2p$, Ga (or As) $3d$, and Au $4f$ photoemission assuming electron IMFP's of 27, 26, and 15 Å, respectively. Also shown in the figure is the GIXPS depth for Ga or As $3d$ photoemission form GaAs at an electron detection angle of 42°.

and As $3d$ photoemission.[14] Also displayed in Fig. 3 are the GIXPS depths for Si $2p$ and Au $4f$ photoemission normal to the surface using Mg $K\alpha$ radiation. The depths plotted in this figure display the enhanced surface sensitivity below the critical angle and illustrate the range of depths that may be probed for typical experimental arrangements and substrate materials.

The total photoelectron flux is determined by integrating Eq. (15) over the entire sample depth:

$$N_q(\phi_0,\theta) = C\frac{D(E_e,E_p)}{\cos\theta}|t_{0,1}|^2 \left[\frac{d\sigma_q}{d\Omega} \right] \rho_q d_{\gamma e} \ ,$$

(17)

where we have introduced the detector-dependent parameter
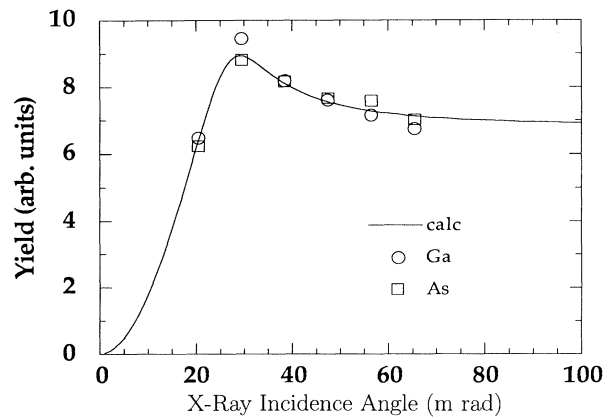
FIG. 4. Calculated GIXPS yield for Mg $K\alpha$ radiation incident on GaAs. The circles and squares are the experimental Ga $3d$ and As $3d$ GIXPS yields, respectively, from an unoxidized GaAs(100) surface. The data have been scaled to the calculated yield.

$$C = I_0 \Omega_d A_d . \tag{18}$$

Displayed in Fig. 4 is the calculated Ga $3d$ (or As $3d$) photoelectron yield for an incident Mg $K\alpha$ beam on a GaAs(100) surface that contains 50% Ga and 50% As termination. The shape of the yield curve is characteristic of that for GIXPS from single-medium materials. The large increase in yield about the critical angle (27 mrad) is a consequence of the enhanced electric field, i.e., $|t_{0,1}|^2 > 1$, in the near-surface region. The decrease in yield at x-ray incidence angles below the critical angle is a result of decreased photon flux density. Above the critical angle, the decreased photoelectron yield is due to the decreased field intensity in the near-surface region. For large incidence angles, $|t_{0,1}|^2 \rightarrow 1$, $d_{\gamma e} \rightarrow \lambda_q \cos\theta$, and the yield approaches that expected from a typical XPS experiment.

C. Grazing-incidence XPS from multilayer media

Calculating the photoelectron yields from multilayer media is a straightforward extension of the results of the previous two sections; Eq. (14) needs only be modified to include reflected electric fields (media 1 to $N-1$) and the possibility of differing electron attenuation factors for the dielectric layers above the layer of interest. Hence, the expression for the differential photoelectron yield from a laminar section of thickness dz in layer $j < N$ may be written as

$$dN_{jq}(\phi_0,\theta,z) = CD(E_{ej},E_p) \left| \frac{d\sigma_{jq}}{d\Omega} \right| \rho_{jq}$$
$$\times \left[\frac{|\mathbf{E}_j^+(z) + \mathbf{E}_j^-(z)|^2}{|\mathbf{E}_0^+(z)|^2} \right]$$
$$\times e^{-\Lambda_{jq}z} \left[\prod_{l=1}^{j-1} e^{-\Lambda_{lq}\Delta_l} \right] dz , \tag{19}$$

where $\Delta_l = d_l - d_{l-1}$ is the thickness of layer l. The total yield that originates in layer j is found by integrating Eq. (19) over the entire thickness of the layer:

$$N_{jq}(\phi_0,\theta) = CD(E_{ej},E_p) \left| \frac{d\sigma_{jq}}{d\Omega} \right|$$
$$\times \rho_{jq} L_{jq}(d_{j-1},d_j) \prod_{l=1}^{j-1} e^{-\Lambda_{lq}\Delta_l} , \tag{20}$$

where

$$L_{jq}(d_{j-1},d_j) = \int_{d_{j-1}}^{d_j} \left[\frac{|\mathbf{E}_j^+(z) + \mathbf{E}_j^-(z)|^2}{|\mathbf{E}_0^+(z)|^2} \right] e^{-\Lambda_{jq}z} dz . \tag{21}$$

Using the electric-field expression of Eq. (8), the right-hand side of Eq. (21) can be evaluated in terms of the normalized field amplitudes $\xi_j^\pm = E_j^\pm / E_0^+$:

$$L_{jq}(d_{j-1},d_j) = \frac{|\xi_j^+|^2 e^{-2k_{jz}''d_{j-1}}}{\Lambda_{jq} + 2k_{jz}''}[1 - e^{-(\Lambda_{jq}+2k_{jz}'')\Delta_j}] + \frac{|\xi_j^-|^2 e^{2k_{jz}''d_{j-1}}}{\Lambda_{jq} - 2k_{jz}''}[1 - e^{-(\Lambda_{jq}-2k_{jz}'')\Delta_j}]$$
$$+ 2\,\mathrm{Re}\left\{ \frac{\xi_j^{+*}\xi_j^- e^{2ik_{jz}'d_{j-1}}}{\Lambda_{jq} - 2ik_{jz}'}[1 - e^{-(\Lambda_{jq}-2ik_{jz}')\Delta_j}] \right\} . \tag{22}$$

This expression is just a sum of complex exponential terms with prefactors that depend on the transmitted and reflected field amplitudes within the layer.

To calculate GIXPS yields from multilayer media, one first determines the electric-field amplitudes within the various media using the formalism developed in Sec. II A. These amplitudes are then used to calculate $L_{jq}(d_{j-1},d_j)$ according to Eq. (22) and this result, along with the appropriate parameters, are inserted into Eq. (20) to determine the photoelectron yield from layer j. To determine the yield from the substrate, i.e., layer N, ξ_j^- is set equal to zero and $\Delta_N \rightarrow \infty$ in Eq. (22).

Calculated Si $2p$ and Au $4f$ photoelectron yields for different Au overlayer thicknesses on a Si substrate are shown in Figs. 5(a) and 5(b), respectively. The calculations were performed for Mg $K\alpha$ radiation and an electron detection angle normal to the surface. An IMFP of 27 Å was used for the Si $2p$ photoelectrons traversing Si while an IMFP of 15 Å was used for both Si and Au photoelectrons in the Au overlayer.[14] Figure 5(a) reveals that as the thickness of the Au overlayer increases, the Si signal decreases with little change in the overall shape of the yield. This decrease in Si signal is due to the attenuation of the Si photoelectrons on passing through the Au overlayer. By 50 Å Au coverage, the Si signal is barely discernable.

In contrast to the Si yields, the changes in the Au yields are much more dramatic as the overlayer thickness is increased. The enhancements in the Au yields around 24 mrad for Au thicknesses less than 10 Å result because the critical angle for Mg $K\alpha$ radiation incident on Si is 24 mrad and the Au overlayers are sufficiently thin that the x-ray attenuation occurs predominantly in the Si substrate. Increasing the Au coverage beyond 10 Å, however, results in a diminution of this feature. For 10-Å Au coverage, a small enhancement in the yield around 55 mrad can be seen. This feature grows with increasing Au thickness and is due to the increased attenuation of the x rays within the Au overlayer. As the Au thickness increases, less radiation reaches the Si and, consequently,

the effects of the supporting substrate become less important in determining the photoelectron yields and the Au yield curves approach that expected from bulk Au.

III. COMPARISON WITH EXPERIMENT

A qualitative analysis of GIXPS data acquired from an as-oxidized GaAs(100) surface has been presented in a previous paper.[8] The large number of parameters required to model this room-temperature oxide precluded a unique structural determination of the oxide overlayer. A simpler system to model, which we have undertaken in the present paper, is the UV oxidized surface that has been annealed at 520 °C. Annealing a UV oxidized surface at 520 °C results in complete desorption of the oxidized As and leaves a surface that is covered with only gallium oxide.[15−17] Determining the structure of this oxide is within the scope of the present paper and provides a stringent test of GIXPS modeling. We have also acquired GIXPS spectra from an unoxidized GaAs(100) surface that was prepared by thermally desorbing all oxides at 600 °C. Modeling the yields from this surface represent a simpler application of GIXPS since there is only one medium to consider, namely, GaAs.

The spectra were acquired using the $K\alpha$ emission from a standard laboratory Mg x-ray source and a double-pass

FIG. 5. Calculated (a) Si $2p$ and (b) Au $4f$ GIXPS yields for different Au overlayer thicknesses (in Å) on Si.

cylindrical mirror analyzer (CMA). The x-ray source was mounted in a housing that allowed the entire source to be rotated about the focal point of the CMA (this was also the center of the sample). The x-ray incidence angle was varied by moving the x-ray tube along this arc, with the sample and CMA position remaining fixed throughout the experiment. For both oxidized and unoxidized surfaces, data were acquired at six different x-ray incidence angles about the critical angle.

A. Unoxidized GaAs(100)

Ga $3d$ (circles) and As $3d$ (squares) GIXPS yields from the unoxidized GaAs(100) surface are displayed in Fig. 4. Also plotted in the figure is the calculated yield (solid line) from a GaAs(100) surface that had 50% Ga and 50% As termination. Aside from scaling, the calculated Ga $3d$ GIXPS yield is the same as the As $3d$ yield because a stoichiometric surface was assumed in the calculation and the IMFP's of both Ga $3d$ and As $3d$ photoelectrons were fixed at 26 Å. Only the Ga and As scaling factors, C_{Ga} and C_{As}, were treated as parameters in fitting the data to the calculated yield.

The Ga $3d$ and As $3d$ data are very similar, and the calculated yield from a stoichiometric surface provides a very good fit to both sets of data. For a truly stoichiometric surface, the fitting parameters C_{Ga} and C_{As} should be the same since they are the same constant in Eq. (17), the equation for the yield from a single medium surface. Using Scofield's total cross sections[18] with corresponding asymmetry parameter corrections,[19] and correcting for the small differences in electron transmission functions of Ga and As $3d$ photoelectrons, we find that C_{Ga} and C_{As} differ by only 5% (Table I). This difference in scaling factors is within experimental error and suggests that the unoxidized surface was nearly stoichiometric over the range of depths probed by GIXPS.

B. Annealed UV oxidized GaAs(100)

Annealing a UV oxidized surface at 520 °C results in a surface that contains only gallium oxide.[15−17] Studies investigating this annealed surface have found that the oxide is composed of Ga in the 3+ oxidation state, indicative of Ga_2O_3. The $3d$ chemical shift of Ga^{3+} is only ∼1 eV, and is too small to enable the oxidized peak to be resolved uniquely from the unoxidized peak in the present study. Nevertheless, the total experimental Ga
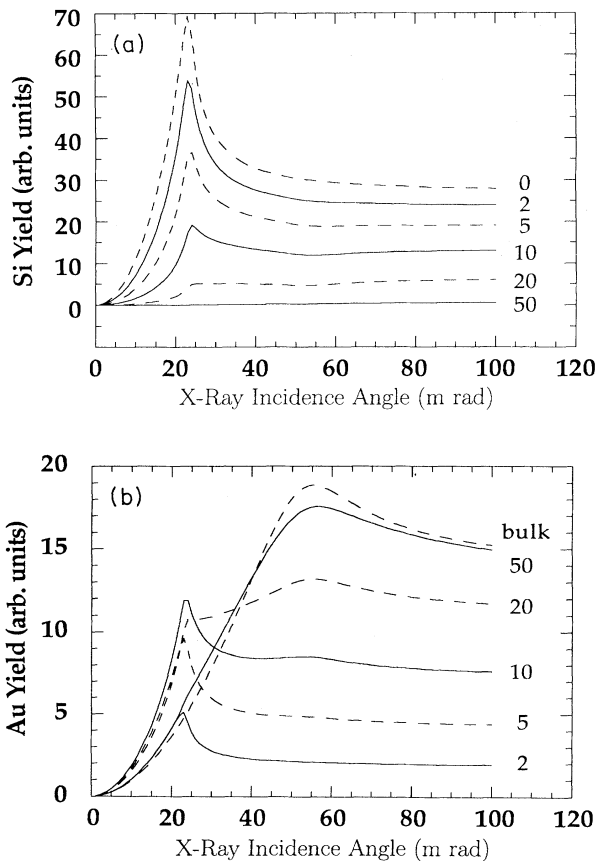
TABLE I. Relative scaling factors (arbitrary units) used to obtain the best fits to the data for the different models discussed in the text.

Model	$C_{Ga\ 3d}$	$C_{As\ 3d}$	$C_{O\ 1s}$
Unoxidized	1.9	1.8	
Oxidized, smooth interface	2.0	3.0	1.8
Oxidized, mixed interface $\lambda_{oxide}=\lambda_{GaAs}$	2.3	2.1	2.1
Oxidized, mixed interface $\lambda_{oxide}=1.1\lambda_{GaAs}$	2.2	1.8	1.9

3d yield can be used to compare with the calculations for different model structures.

Ga 3d, As 3d, and O 1s GIXPS yields acquired from the 520 °C annealed oxidized surface are presented in Figs. 6(a), 6(b), and 6(c), respectively. As a first attempt at fitting the data, we assumed that the interface between the oxidized surface and the GaAs substrate was smooth and that the oxide overlayer was of uniform composition. The data were modeled by varying the oxide composition, density, and thickness. Due to the lack of information on photoelectron IMFP's in gallium oxide, the IMFP's of the photoelectrons traversing the oxide overlayer were assumed to be the same as those for the GaAs substrate, namely, 26 Å for Ga 3d and As 3d photoelectrons and 17 Å for O 1s photoelectrons.[14] The model that provides the best fit to the data,[20] illustrated in Fig. 7(a), consists of 20 Å of $Ga_2O_{3.5}$ having a density of 6.5 g/cm^3. While the density of this model is comparable to that of the hexagonal Ga_2O_3 phase, 6.44 g/cm^3,[21] the model oxide contains more oxygen than is stoichiometric.

The fits to the data are plotted as dashed lines in Figs. 6(a)–6(c). The Ga 3d and O 1s fits represent the data reasonably well, but the As 3d fit is poor. The calculated As 3d GIXPS yield does not display the characteristic enhanced yield about the critical angle. The shape of the calculated As 3d yield is a result of the thick oxide overlayer through which the As 3d photoelectrons must traverse before exiting the sample. The Ga oxide layer is sufficiently thick that the enhanced electric field about the critical angle does not penetrate into the GaAs substrate, and consequently, the number of As 3d photoelectrons is smaller than if the oxide were not present. As the x-ray incidence angle is increased, the x-ray flux density increases in the GaAs substrate and the calculated As 3d photoelectron yield increases. This yield then levels off as the x-ray penetration depth becomes much larger than the electron IMFP. Comparison of As 3d model yield with the data, therefore, indicates that the model oxide is too thick. Further support for an overestimated oxide thickness comes from the As 3d scaling factor (see Table I). For the smooth interface model depicted in Fig. 7(a), C_{As} is about 50% larger than the corresponding Ga 3d, O 1s, and unoxidized Ga and As scaling factors. Referring to Eq. (20), the implication of such a large scaling factor is that the calculated As 3d yield is too small, or equivalently, more As 3d is detected than is accounted for by the model.

The above results imply that there must be more As closer to the surface. There are several different models that one can propose to increase the amount of As near the surface, including adding As to the surface, creating an As-rich oxide-GaAs interface, and by introducing a rough interface whereby the oxide thickness is shallower in some regions than in others. We have evaluated these possibilities, and the first two, adding excess As at the surface and at the interface, do not improve the model fits significantly. This is not surprising since the inclusion of excess As at the surface predominantly scales the data without significantly changing the shape of the calculated As 3d yield. Similarly, adding excess As at the interface increases the overall yield, but fits the As 3d yield poorly

because excess As at the interface is seen primarily at the large incidence angles where the x-ray attenuation in the oxide overlayer is less.

The modeling formalism developed earlier in this paper assumed that the interfaces between the media were perfectly planar. As an approximation to a model with a rough interface, we have added a layer uniformly com-
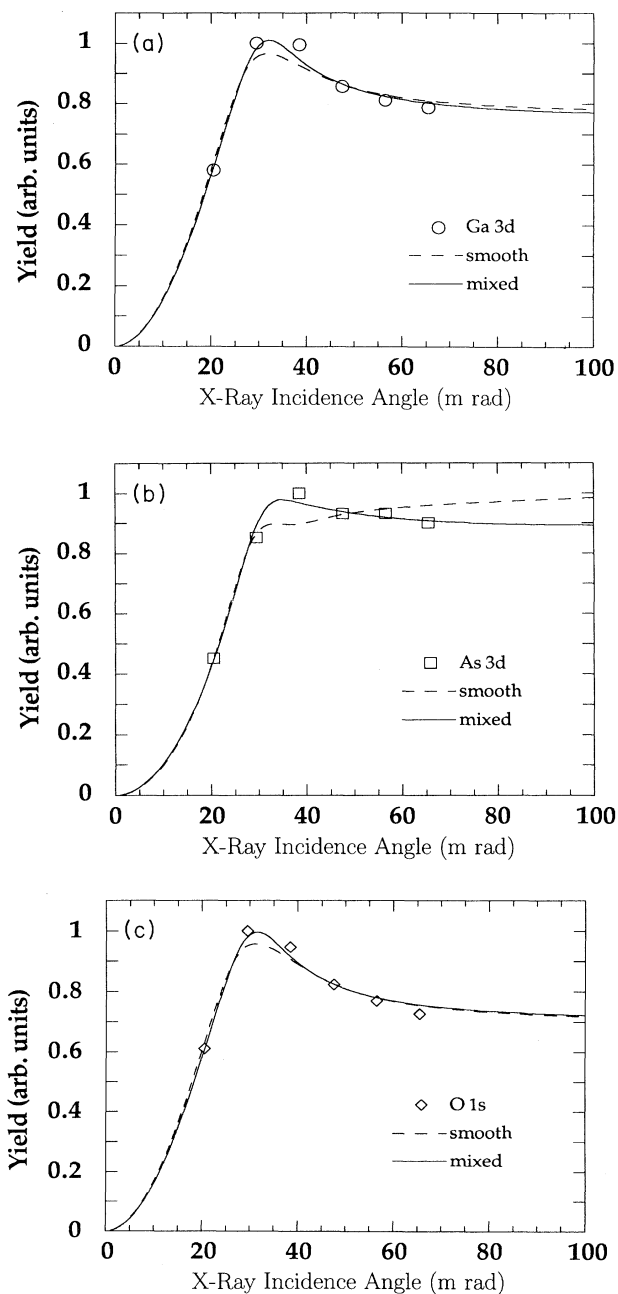
FIG. 6. (a) Ga 3d, (b) As 3d, and (c) O 1s GIXPS data (shown as open symbols) from a UV oxidized GaAs(100) surface that was annealed in vacuum at 520 °C for 10 min. Dashed curves are the fits to the data for the smooth interface model depicted in Fig. 7(a) and the solid lines are the fits for the mixed interface model shown in Fig. 7(b).

(a)

(b)
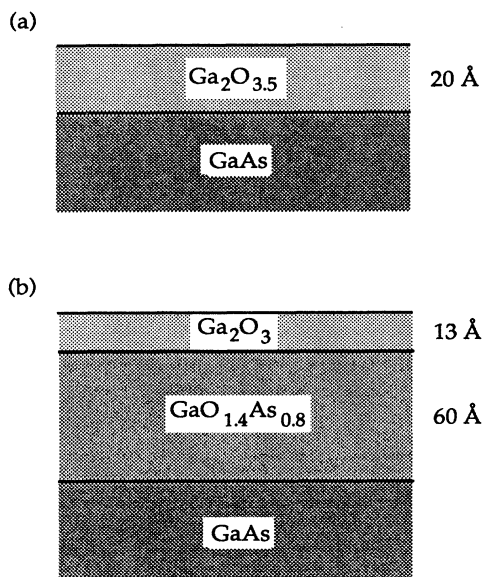
FIG. 7. (a) Smooth interface and (b) mixed interface models that provide the best fits to the experimental GIXPS data from the 520 °C annealed, oxidized GaAs(100) surface.

posed of Ga, As, and O, i.e., GaO_xAs_y, between the gallium oxide and the GaAs substrate. The stoichiometry of this interfacial region as well as the density and thickness of the layer were treated as fitting parameters. The model that best described the data is illustrated in Fig. 7(b). The oxide overlayer is composed of 13 Å of Ga_2O_3 having a density of 6.0 g/cm^3 and the interfacial region contains 60 Å of $GaO_{1.4}As_{0.8}$ having a density also of 6.0 g/cm^3. The oxide composition that emerges from this model is consistent with the findings of previous studies[8,15,16] and the density is within the range of densities reported for the various Ga_2O_3 phases.[21] Essentially the same structural parameters were obtained for interfacial thicknesses that were 10 Å thinner or thicker. The relative insensitivity of the fits to this parameter are consequences of the thick oxide, both Ga_2O_3 and $GaO_{1.4}As_{0.8}$, and the nearly equal concentrations of Ga and As in the interfacial region. Similarly, the fits are relatively insensitive to errors in electron IMFP's in the oxide.

The best fits to the data for the mixed interface model are plotted as solid lines in Figs. 6(a)–6(c). From these figures it can be seen that the calculated yields describe the data very well. The gallium oxide thickness for this model is only 13 Å, considerably smaller than that for the smooth oxide model. It is this reduction in oxide thick-

ness along with the incorporation of As into a rough interfacial layer that results in a calculated As $3d$ GIXPS yield that contains the observed enhancement about the critical angle. The scaling factors for the best mixed interface model are very similar to each other, but are about 15% larger than those obtained from the unoxidized surface (Table I). Better agreement between the unoxidized and oxidized scaling factors can be obtained by increasing the IMFP's of the electrons in the oxide overlayer. Given that the electron IMFP's in the oxide were assumed to be the same as those in GaAs, a 10% increase in these values is certainly plausible. Furthermore, the optimal structural parameters do not change significantly if these IMFP's are increased by 10%.

The presence of a rough interfacial region between the gallium oxide and the GaAs substrate is not surprising. An as-oxidized GaAs surface contains both arsenic and gallium oxides. When this surface is annealed at ~500 °C, as was done in the present paper, the desorption of oxidized As occurs via dissociation of the arsenic oxide, with some of the O being transferred to unoxidized Ga.[17,22,23] Such a mechanism requires the consumption of the GaAs substrate, and given the likely inhomogeneity of the as-oxidized surface as well as nonuniform local heating, it would be surprising if the interface were smooth. Hence, the model that we propose for this annealed oxide surface is consistent with existing studies.

IV. SUMMARY AND FUTURE DIRECTIONS

In this paper we have presented an algorithm for computing GIXPS yields from thin films consisting of an arbitrary number of dielectric media. We have used this algorithm to model data from an unoxidized GaAs(100) surface and from an annealed, UV oxidized GaAs(100) surface. The unoxidized surface was found to be nearly stoichiometric. The best fit model for the annealed, oxidized surface contained a Ga_2O_3 oxide overlayer and a rough interface between the oxide and GaAs substrate. The good agreement between model fits and experimental data demonstrate that GIXPS is a valuable tool for nondestructive depth profiling that is amenable to quantitation. We believe that GIXPS will be applicable to a variety of problems, including the determination of overlayer thickness, concentration profiles of thin films (both metal and oxide), and monitoring the diffusion of species between media.

ACKNOWLEDGMENTS

*Present address: Department of Physics, Mansfield University, Mansfield, PA 16933.

[1]C. S. Fadley and S. Å. L. Bergström, Phys. Lett. 35A, 375 (1971).

[2]W. A. Fraser, J. V. Florio, W. N. Delgass, and W. D. Robertson, Surf. Sci. 36, 661 (1973).

[3]C. S. Fadley, R. J. Baird, W. Siekhaus, T. Novakov, and S. Å.

L. Bergström, J. Electron Spectrosc. Relat. Phenom. 4, 93 (1974).

[4]B. L. Henke, Phys. Rev. A 6, 94 (1972).

[5]M. Mehta and C. S. Fadley, Phys. Lett. 55A, 59 (1975).

[6]M. Mehta and C. S. Fadley, Chem. Phys. Lett. 46, 225 (1977).

[7]J. Kawai, M. Takami, M. Fujinami, Y. Hashiguchi, S. Hayakawa, and Y. Gohshi, Spectrochim. Acta, Part B 47, 983

(1992).

[8]M. J. Chester, T. Jach, and S. Thurgate, J. Vac. Sci. Technol. B **11**, 1609 (1993).

[9]L. G. Parratt, Phys. Rev. **95**, 359 (1954).

[10]D. K. G. de Boer, Phys. Rev. B **44**, 498 (1991).

[11]This is not a physical restriction in the following formulas, but rather a restriction to simplify the notation.

[12]A. H. Compton and S. K. Allison, *X-Rays in Theory and Experiment* (Van Nostrand, New York, 1935).

[13]B. L. Henke, P. Lee, T. J. Tanaka, R. L. Shimabukuro, and B. K. Fujikawa, At. Data Nucl. Data Tables **27**, 1 (1982).

[14]S. Tanuma, C. J. Powell, and D. R. Penn, Surf. Interf. Anal. **17**, 927 (1991).

[15]S. Ingrey, W. M. Lau, and N. S. McIntyre, J. Vac. Sci. Technol. A **4**, 984 (1986).

[16]W. M. Lau, R. N. S. Sodhi, and S. Jin, J. Vac. Sci. Technol. B **8**, 1899 (1990).

[17]M. J. Chester, T. Jach, and J. A. Dagata, J. Vac. Sci. Technol. A **11**, 474 (1993).

[18]J. H. Scofield, J. Electron Spectrosc. Relat. Phenom. **8**, 129 (1976).

[19]R. F. Reilman, A. Msezane, and S. T. Manson, J. Electron Spectrosc. Relat. Phenom. **8**, 389 (1976).

[20]To measure the quality of fit between calculated and experimental yields for each photoelectron spectrum, a scaled R factor was used:

$$R_q = \frac{100}{N} \left\{ \sum_{i=1}^{N} \left[\frac{Y_{\mathrm{exp}} - cY_{\mathrm{calc}}}{Y_{\mathrm{exp}}} \right]^2 \right\}^{1/2} ,$$

where Y_{exp} (Y_{calc}) is the measured (calculated) yield, N is the number of incidence angles, and c is the scaling factor discussed in the text. The total R factor for a given model structure was then determined by the relation

$$R_T = \frac{1}{M} \left[\sum_{q}^{M} R_q^2 \right]^{1/2} ,$$

where M was the number of photoelectron spectra under consideration.

[21]*CRC Handbook of Chemistry and Physics,* 71st ed., edited by D. R. Lide (CRC, Boca Raton, 1990).

[22]R. W. Grant, S. P. Kowalczyk, J. R. Waldrop, and W. A. Hill, in *Physics of MOS Insulators,* edited by G. Lucovsky, S. T. Pantelides, and T. J. Galeener (Pergamon, New York, 1980), p. 202.

[23]C. D. Thurmond, G. P. Schwartz, G. W. Kammlott, and B. Schwartz, J. Electrochem. Soc. **127**, 1366 (1980).